NANO LETTERS

pubs.acs.org/NanoLett

Letter

Flexoelectric Enhancement of Strain Gradient Elasticity Across a Ferroelectric-to-Paraelectric Phase Transition

Varun Harbola,* David Pesquera, Ruijuan Xu, Paul D. Ashby, Lane W. Martin, and Harold Y. Hwang

Cite This: *Nano Lett.* 2024, 24, 10331−10336

Read Online

ACCESS | Metrics & More | Article Recommendations | Supporting Information

ABSTRACT: We study the temperature dependent elastic properties of $Ba_{0.8}Sr_{0.2}TiO_3$ freestanding membranes across the ferroelectric-to-paraelectric phase transition using an atomic force microscope. The bending rigidity of thin membranes can be stiffer compared to stretching due to strain gradient elasticity (SGE). We measure the Young's modulus of freestanding $Ba_{0.8}Sr_{0.2}TiO_3$ drumheads in bending and stretching dominated deformation regimes on a variable temperature platform, finding a peak in the difference between the two Young's moduli obtained at the phase transition. This demonstrates a dependence of SGE on the dielectric properties of a material and alludes to a flexoelectric origin of an effective SGE.

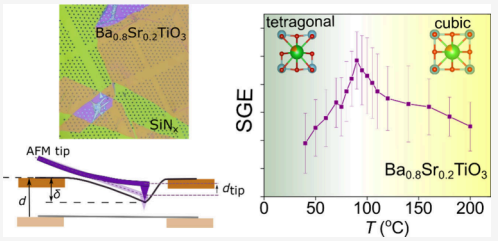

KEYWORDS: *Oxides, Ferroelectric, Nanomechanics, Flexoelectricity, Nonlinear elasticity*

Conventional mechanical response of materials is usually described using linear elastic theory which is a local theory and does not include any nonlinear or nonlocal contributions. In this framework, the Young's modulus E and the Poisson's ratio ν are used to calculate the deformation response of a material geometry upon loading. Strain gradient elasticity (SGE) is a nonlinear and nonlocal extension of elastic theory by including energetic contributions from strain gradients,[1,2] which can become important while considering nanomaterials and nanodevices where strain gradients can be large upon deformation.[2] SGE thus extends the notion of elasticity by not only adding nonlinearity, but also nonlocality as strain gradients are intrinsically nonlocal in nature. For a material with SGE, the total elastic energy density ϕ upon deformation is given by

$$\phi = \frac{1}{2}E\varepsilon^2 + \frac{1}{2}K|\nabla\varepsilon|^2 \quad (1)$$

where E is the Young's modulus, ε is the strain, and K is the strain gradient elastic coupling coefficient.

The origin of SGE is still an open question, and conventional materials have been argued to have a diminishingly small strain gradient response.[3] In our previous work, however, while measuring the elastic response in sub-100 nm-thick $SrTiO_3$ membranes, it was observed that at the length scales of ∼10 nm, the SGE contribution to elasticity is not just perturbative, but on par with the linear elastic response.[4] Deducing the origin of the SGE response still remained elusive. One of the proposed mechanisms to make SGE relevant for geometries at the nanoscale is flexoelectricity,[5−7] which refers to the induced polarization in a material subjected to a strain gradient.[8−12] Using this connection between SGE and flexoelectricity, the flexoelectric response coefficients for $SrTiO_3$ were inferred from the mechanical response.[4] Naturally, this leads to the question, is there a more direct way to measure the connection between flexoelectricity and SGE? To answer this, we scrutinize flexoelectricity in materials and how it links to an effective SGE more closely.

Since strain gradients break centrosymmetry, flexoelectric polarization is universal irrespective of the underlying lattice structure (i.e., flexoelectricity is governed by a fourth-rank tensor and is thus present in all materials, but it is significantly stronger in high-K dielectrics[11]). Flexoelectricity has been measured in a variety of materials,[13−18] but in the past decade, with advances in nanofabrication, flexoelectricity in at the nanoscale has been well characterized,[19−21] where owing to the small dimensions, strain gradients can be large. In oxide membranes, flexoelectricity has been observed to affect the polarization profile of $BaTiO_3$[22] and $BiFeO_3$[23] upon bending, domain-wall motion in $PbZr_{0.2}Ti_{0.8}O_3$[24] and even photoconductance in $BiFeO_3$.[25] To characterize flexoelectricity, the canonical parameter is μ, the flexoelectric coefficient which is defined as the change in polarization P of a material when exposed to a unit strain gradient. The parameter μ is directly related to the flexocoupling coefficient of the material f via the dielectric constant χ by $\mu = \chi f$, as f is the proportionality coefficient between the strain gradient and the electric field introduced in the material. This dependency of the flexo-

Received: June 21, 2024
Revised: August 2, 2024
Accepted: August 7, 2024
Published: August 12, 2024

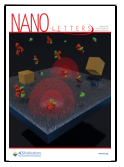

https://doi.org/10.1021/acs.nanolett.4c02946
Nano Lett. 2024, 24, 10331−10336

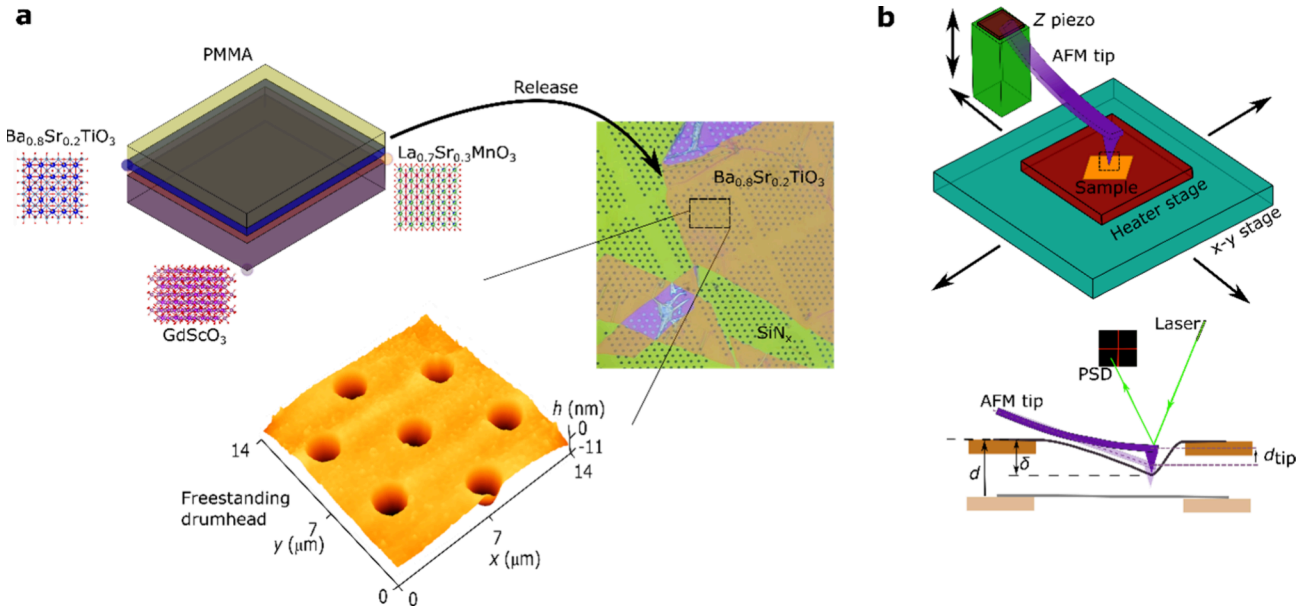

Figure 1. Making freestanding drumheads and measuring them. (a) A schematic of the as-grown heterostructure coated with PMMA is shown before release. After release, an optical micrograph and a 3D rendered AFM topography image are shown to clearly display the freestanding drumheads. (b) A representation of the AFM measurement on a heater stage and the bottom panel shows all relevant parameters to measure the mechanical response of a freestanding drumhead.

electric effect on the dielectric susceptibility has been previously established in many materials.[17,18,26,27] Thus, relating the polarization energy density upon bending to SGE,[4] we find that

$$K = \chi f^2 \tag{2}$$

This shows that the SGE coefficient K is proportional to the dielectric constant of the material as long as the flexocoupling coefficient f remains the same.

Recent work has shown that the stiffness of a ferroelectric material can be altered by a combination of polarization and the flexoelectric effect.[28] As discussed above, in $SrTiO_3$ membranes, an SGE response was observed with an implied coupling to the flexoelectricity.[4] The flexoelectric contribution to deformation energy results in a higher inferred elastic modulus from a bending dominant deformation (E_{lin}) as compared to that inferred from a stretching dominant deformation (E_{cub}).[4,5] This difference between bending and stretching elasticity can be quantified by

$$E_{lin} - E_{cub} = \frac{12\chi f^2}{t^2} \tag{3}$$

This relies on the fact that a uniform strain gradient is present across the material as it is bent, which is proportional to the maximum strains at the free boundaries and inversely proportional to the thickness. Consequently, as long as the sample is experiencing pure bending deformation (i.e., neutral axis has 0 strain), this relation will hold regardless of the actual magnitude of the strain and strain gradients. Furthermore, the difference between the two moduli is also linearly dependent on the dielectric susceptibility of the material for SGE rooted in flexoelectricity. This stiffening of the gradient elastic response rooted in a nonlocal strain driven polarization draws parallels to the stiffening of the elastic response in piezoelectric materials through a local strain driven polarization.[29]

Thus, to measure the direct effect of dielectric properties and flexoelectricity on SGE, we need a material where the dielectric properties change significantly as a function of some controllable parameter. When a ferroelectric material goes through a ferroelectric-to-paraelectric phase transition, the dielectric permittivity diverges at the transition temperature in the bulk limit. Therefore, such materials are ideal for exploring the effect of flexoelectricity on the bending rigidity through a temperature dependent elastic measurement. Such materials should also be thin enough to have a significant effect of SGE on the mechanical properties, as that contribution is inversely dependent on the square of the thickness. Recent developments in thin-film growth have made it possible to grow high quality single-crystalline oxide thin-film heterostructures and membranes with a variety of physical properties.[22,30−33] In this work we use freestanding $Ba_{0.8}Sr_{0.2}TiO_3$ membranes due to the proximity of its ferroelectric-to-paraelectric phase transition above room temperature.[34,35] These membranes were prepared by growing a thin film of $Ba_{0.8}Sr_{0.2}TiO_3$ using pulsed laser deposition (PLD) with a buffer layer of $La_{0.7}Sr_{0.3}MnO_3$ on a $GdScO_3$ (110) substrate (Figure 1a). The buffer layer was then dissolved using a solution of potassium iodide in hydrochloric acid and water (Figure 1).[35,36] After the buffer layer was etched, the $Ba_{0.8}Sr_{0.2}TiO_3$ membrane was transferred onto a SiN_x grid with an array of 2 μm diameter holes to form freestanding drumheads. This is similar to the drumhead geometry used to study several other materials including graphene,[37,38] MoS_2,[39] $SrTiO_3$[4,40] and $NaNbO_3$.[41] An atomic force microscope (AFM) topography scan of these drumheads is shown (Figure 1a).

Here, we use the AFM to measure the elastic properties of these freestanding $Ba_{0.8}Sr_{0.2}TiO_3$ drumheads. Such a measurement protocol was developed to measure the elastic properties of 2D materials,[37−39] particulars of the measurement used in this paper have been described in detail elsewhere with a similar measurement setup on $SrTiO_3$.[4] The radius of the tip used is ∼15 nm (Multi75DLC from BudgetSensors), which is

https://doi.org/10.1021/acs.nanolett.4c02946
Nano Lett. 2024, 24, 10331−10336

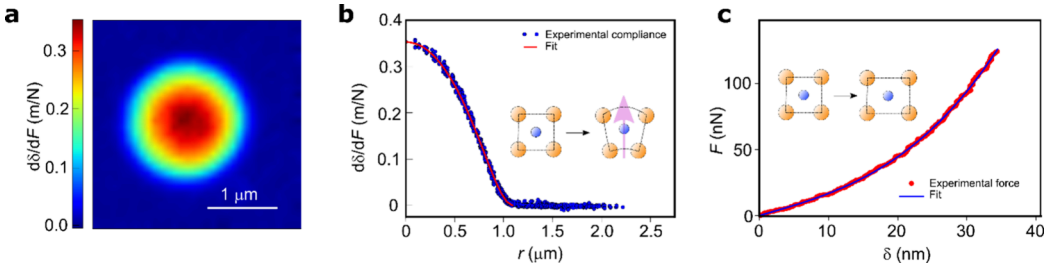

Figure 2. Extracting the bending and stretching rigidity of freestanding drumheads. (a) A 32 × 32 pixel force map taken on and around a drumhead and the compliance from the perturbative linear response is plotted as a function of spatial position, after subtracting out the compliance of the neighboring SiN_x membrane. (b) The compliance from linear response plotted as a function of distance from the center of the drumhead (blue dots) and a fit to the Euler−Bernoulli compliance obtained by solving and iterating over eq 4. (c) The nonlinear nature of the $F-\delta$ curve due to the predominance of stretching at higher forces. The fit is to the cubic force response equation (eq 5), and the coefficient of the cubic response is used to evaluate E_{cub}.

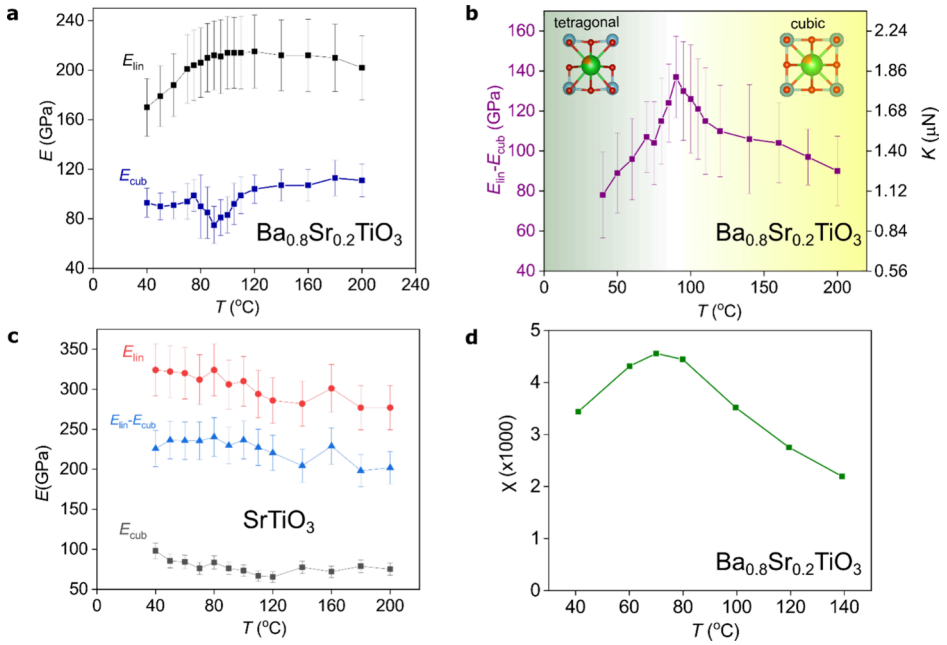

Figure 3. Measured elastic moduli for freestanding drumheads. (a) Average E_{lin} and E_{cub} of seven $Ba_{0.8}Sr_{0.2}TiO_3$ freestanding drumheads with temperature varying from 40 to 200 °C. E_{cub} shows a clear dip at the phase transition temperature, as expected at a structural phase transition. By contrast E_{lin} varies smoothly across this temperature range. Error bars indicate the error in measuring the spring constant of the AFM tip by the thermal method[42] and the standard deviation over the 7 data sets. (b) The difference between the two measured moduli shows a peak at the transition temperature. This peak also corresponds to a peak in the dielectric response of the material as it goes through a paraelectric−ferroelectric phase transition. This shows a dependence of the SGE coefficient K and the dielectric properties of $Ba_{0.8}Sr_{0.2}TiO_3$ and hence flexoelectricity. (c) Control experiment on the same temperature range as that for $Ba_{0.8}Sr_{0.2}TiO_3$ but on $SrTiO_3$ which does not have a phase transition. We can see no dip-like features in either E_{lin} or E_{cub} nor a peak appearing in the difference $E_{lin} - E_{cub}$ as was seen in the case of $Ba_{0.8}Sr_{0.2}TiO_3$. The error bars respresent the same errors as in (a). (d) The permittivity measurement of a 100 nm thick $Ba_{0.8}Sr_{0.2}TiO_3$ showing the peak in dielectric response, cutoff by finite thickness effects, at the phase transition, measured on circular capacitor structures defined on the thin film via dry etching. Adapted with permission from ref 35. Copyright 2020 John Wiley and Sons.

much smaller compared to the radius of the drumhead (1 μm) and a diamond-like-carbon coated tip is used for the measurement to prevent it from wearing during the experiment. This wear resistance was previously confirmed even at much higher forces which were used to break oxide membrane drumheads.[40] Different from that previous work, this measurement was conducted using a variable temperature stage on the AFM (Figure 1b). This enables elastic measurements across a range of temperatures ranging from 40 to 200 °C, which encompasses the phase-transition temperature established previously.[35] Once the drumhead of choice has been identified, we produce a force−distance ($F-d$) map on a 32 × 32 pixel array on and around the drumhead area. Note that for all measurements, the force constant of the AFM tip being used is measured using the thermal method.[42] This $F-d$ map can be turned into a force-deflection ($F-\delta$) map by subtracting the response of the cantilever and the SiN_x film. The details on the exact steps for doing this have been published previously.[4] Once we have the $F-\delta$ map, we can map the compliance of the drumhead ($\partial\delta/\partial F$) as a function of position, giving us a compliance map (Figure 2a). For a 13 nm-thick membrane of $Ba_{0.8}Sr_{0.2}TiO_3$, we can probe both the linear and nonlinear $F-\delta$ response of the drumheads by varying the applied force. The linear $F-\delta$ response regime for lower forces (below 10 nN) captures the perturbative bending dominated deformation of the membrane from its equilibrium position. Similarly, the

https://doi.org/10.1021/acs.nanolett.4c02946
Nano Lett. 2024, 24, 10331−10336

nonlinear regime of the $F-\delta$ response arises due to geometric nonlinearities in the membrane deformation implying a more stretching dominated deformation.[4] To extract the Young's modulus E_{lin} from the linear $F-\delta$ response, we use numerical solutions of the Euler−Bernoulli bending equation for a clamped plate with uniform cross section, the general form of which is given by

$$\frac{E_{lin}t^3}{12(1-\nu^2)}\nabla^4 u(r,\theta) - T\nabla^2 u(r,\theta) = \rho(r,\theta) \quad (4)$$

to fit to the experimental compliance as a function of radial distance from the center of the drumhead (Figure 2b). Here, E_{lin} captures the elastic response of the material upon bending, as defined above, t is the thickness, T is the pretension, u is the deflection profile of the drumhead, and is the ρ is thepressure profile of the load applied. The free parameters for this fit are E_{lin} and T. For nonlinear response, the Young's modulus for a stretching dominated response, E_{cub}, is obtained by fitting the $(F-\delta)$ curve to a cubic response upon central point loading (Figure 2c), given by

$$F(\delta) = \frac{4\pi E_{lin}t^3}{3(1-\nu^2)R^2}\delta + \pi T\delta + \frac{cE_{cub}t}{R^2}\delta^3 \quad (5)$$

The lattice deformation mechanisms that E_{cub} and E_{lin} represent in terms of rigidity are different. More details on handling the raw data and its analysis are shown in Supporting Information Figure S2. Since E_{lin} captures the bending response, there is a built-in strain gradient, and thus this modulus is affected by SGE. For a stretching deformation, there is no significant strain gradient, and thus E_{cub} is nominally not affected by SGE. Note that E_{lin} and E_{cub} are not calculated from a nonlocal model completely capturing the free energy minimization of eq 1, but rather by appropriate extension of local elastic theories in bending and stretching dominated deformation regimes, the details of which are discussed in our previous work on $SrTiO_3$.[4]

We studied how the mechanical stiffness for the two different stretching- and bending-dominated deformations evolve with temperature by looking at the moduli inferred from linear (E_{lin}) and cubic (E_{cub}) responses, separately, across the studied temperature range. The temperature traces are taken over seven different holes. At each temperature, we let the sample equilibrate for more than 20 min which is much longer than the time constant of equilibration of our sample and then measure the mechanical response (Figure 3a) (see Supporting Information Figure S1). We first observe that the $E_{lin} > E_{cub}$ at all measured temperatures. Generally, for materials undergoing a ferroelectric-to-paraelectric phase transition, as they also go through a structural phase transition changing the lattice symmetry, the material becomes less stiff at the transition temperature as the lattice has to accommodate a structural change.[43,44] We observe a similar drop in E_{cub} around 85 °C showing a softening of the elastic response for stretching near the phase transition (Figure 3a). However, such softening is absent on the temperature trace of E_{lin}, signifying a smooth variation of the bending stiffness across this temperature range. These same trends can be observed in each individual trace of each hole (see Supporting Information Figure S3). Note that another effect, which is the electromechanical coupling coefficient peaking at the paraelectric-to-ferroelectric phase transition,[45,46] can possibly be used to consider our data. The electromechanical coupling parameter directly relates how efficiently the mechanical energy of a strained material manifests itself as electrical energy through polarizations. This coupling also peaks near the paraelectric-ferroelectric transition. However, the electromechanical coupling would affect bending and stretching in the same manner, as it is a local effect and would not differentiate between different deformation regimes. Thus, we can rule this out as a dominant contribution. This implies that the intrinsic bending rigidity varies smoothly across the phase transition of $Ba_{0.8}Sr_{0.2}TiO_3$, while the stretching rigidity response shows a dip. The difference between bending and stretching rigidity is governed directly by SGE (eq 3), thus showcasing that SGE contribution is essentially being enhanced across the phase transition. This is apparent when we plot the difference $E_{lin} - E_{cub}$ as a function of temperature (Figure 3b), and a peak can be seen at the phase-transition temperature. We note here that across the phase transition the relative change in the flexocoupling coefficient f, through Kogan's estimate,[8] would be of the order of the relative change in the lattice parameter a ($\Delta f/f \sim \Delta a/a$), which means for the change in the flexoelectric coefficient μ across the phase transition, f is effectively constant as compared to the change in the dielectric constant. We also performed a similar experiment on $SrTiO_3$ as a control, as it does not have a phase transition in this temperature range. We did not observe any dip-like features and both E_{lin} and E_{cub} decrease monotonically with increase in temperature (Figure 3c). Comparing our results for $Ba_{0.8}Sr_{0.2}TiO_3$ to the connection between SGE and flexoelectricity and knowing that the dielectric response peaks at the ferroelectric-to-paraelectric phase transition[35] (Figure 3d), this finding clearly demonstrates a dependence of SGE on the dielectric response of the material and hence flexoelectricity. The slight difference between the phase transition temperature observed in the dielectric measurement and through our mechanical measurement can be attributed to the different thicknesses of membranes used (100 nm in the capacitive measurement versus 13 nm for mechanical measurement) and the difference in the strain state due to the presence of 40 nm thick electrodes for the dielectric measurement.[35]

With the interest in flexoelectricity growing recently, this work showcases the flexoelectric influence on the elastic moduli of materials, not just on the polarization response of the material. This finding provides significant insights for the future studies and applications of oxide materials in nano-electromechanical/microelectromechanical systems (NEMS/MEMS). Our finding shows that at the nanoscale the mechanical properties for certain materials can be tuned via the dielectric response, opening possibilities for fine control over material rigidity using dielectric tuning parameters such as temperature and electric field. Furthermore, our technique can probe a phase transition in a thin membrane material where a capacitive measurement of the dielectric constant is extremely challenging and perturbative. To conclude, we measured the temperature dependent elastic properties of freestanding $Ba_{0.8}Sr_{0.2}TiO_3$ membranes in bending and stretching dominated deformation regimes and found that the enhancement of the bending rigidity with respect to the stretching rigidity was highly temperature dependent. Across a ferroelectric-to-paraelectric phase transition, the SGE response is peaked at the transition temperature, showing a clear dependence of SGE on the dielectric properties of the material. This strongly indicates that the origin of this effective SGE response is flexoelectric in nature.

https://doi.org/10.1021/acs.nanolett.4c02946
Nano Lett. 2024, 24, 10331−10336

■ ASSOCIATED CONTENT

Supporting Information

The Supporting Information is available free of charge at https://pubs.acs.org/doi/10.1021/acs.nanolett.4c02946.

Figures and discussions pertaining to obtaining the time constant for the temperature dependent measurement, analysis of data, and individual data traces for all the 7 drumheads measured (PDF)

■ AUTHOR INFORMATION

Corresponding Author

Varun Harbola − *Department of Physics, Stanford University, Stanford, California 94305, United States; Stanford Institute of Materials and Energy Sciences, SLAC National Laboratory, Menlo Park, California 94025, United States;* Present Address: Max Planck Institute for Solid State Research, Heisenbergstr. 1, 70569 Stuttgart, Germany; orcid.org/0000-0002-5485-762X; Email: v.harbola@fkf.mpg.de

Authors

David Pesquera − *Department of Materials Science and Engineering, University of California, Berkeley, Berkeley, California 94720, United States; Catalan Institute of Nanoscience and Nanotechnology (ICN2), CSIC and BIST, 08193 Barcelona, Spain;* orcid.org/0000-0003-0681-3371

Ruijuan Xu − *Stanford Institute of Materials and Energy Sciences, SLAC National Laboratory, Menlo Park, California 94025, United States; Department of Applied Physics, Stanford University, Stanford, California 94305, United States; Department of Materials Science and Engineering, North Carolina State University, Raleigh, North Carolina 27606, United States;* orcid.org/0000-0001-5046-0599

Paul D. Ashby − *Molecular Foundry, Lawrence Berkeley National Lab, Berkeley, California 94720, United States;* orcid.org/0000-0003-4195-310X

Lane W. Martin − *Department of Materials Science and Engineering, University of California, Berkeley, Berkeley, California 94720, United States; Materials Sciences Division, Lawrence Berkeley National Lab, Berkeley, California 94720, United States; Departments of Materials Science and NanoEngineering, Chemistry, and Physics and Astronomy and the Rice Advanced Materials Institute, Rice University, Houston, Texas 77005, United States*

Harold Y. Hwang − *Stanford Institute of Materials and Energy Sciences, SLAC National Laboratory, Menlo Park, California 94025, United States; Department of Applied Physics, Stanford University, Stanford, California 94305, United States*

Complete contact information is available at: https://pubs.acs.org/10.1021/acs.nanolett.4c02946

Notes

The authors declare no competing financial interest.

■ ACKNOWLEDGMENTS

This work was supported by the U.S. Department of Energy, Office of Basic Energy Sciences, Division of Materials Sciences and Engineering (Contract No. DE-AC02-76SF00515) and the Gordon and Betty Moore Foundation's Emergent Phenomena in Quantum Systems Initiative (Grant No. GBMF9072, synthesis equipment). For work completed at Berkeley, D.P. acknowledges the National Science Foundation under Grant DMR-2329111. D.P. further acknowledges the support of the European Union's Horizon 2020 research and innovation programme under Grant agreement No. 797123 (Marie Skłodowska-Curie FERROENERGY) and funding from "la Caixa" Foundation fellowship (ID 100010434). The ICN2 is funded by the CERCA programme/Generalitat de Catalunya and by the Severo Ochoa Centres of Excellence Programme, funded by the Spanish Research Agency (AEI, CEX2021-001214-S). L.W.M. acknowledges support of the Army Research Office under Grant W911NF-21-1-0118. R.X. acknowledges the support from the Faculty Research and Professional Development Program (FRPD) at North Carolina State University. Work at the Molecular Foundry was supported by the Office of Science, Office of Basic Energy Sciences, of the U.S. Department of Energy under Contract No. DE-AC02-05CH11231.

■ REFERENCES

(1) Mindlin, R. D. Micro-Structure in Linear Elasticity. *Arch. Ration. Mech. Anal.* **1964**, *16*, 51−78.

(2) Lam, D. C. C.; Yang, F.; Chong, A. C. M.; Wang, J.; Tong, P. Experiments and Theory in Strain Gradient Elasticity. *J. Mech. Phys. Solids* **2003**, *51*, 1477−1508.

(3) Maranganti, R.; Sharma, P. A Novel Atomistic Approach to Determine Strain-Gradient Elasticity Constants: Tabulation and Comparison for Various Metals, Semiconductors, Silica, Polymers and the (Ir) Relevance for Nanotechnologies. *J. Mech. Phys. Solids* **2007**, *55* (9), 1823−1852.

(4) Harbola, V.; Crossley, S.; Hong, S. S.; Lu, D.; Birkhölzer, Y. A.; Hikita, Y.; Hwang, H. Y. Strain Gradient Elasticity in $SrTiO_3$ Membranes: Bending versus Stretching. *Nano Lett.* **2021**, *21* (6), 2470−2475.

(5) Majdoub, M. S.; Sharma, P.; Cagin, T. Enhanced Size-Dependent Piezoelectricity and Elasticity in Nanostructures Due to the Flexoelectric Effect. *Phys. Rev. B* **2008**, *77* (12), 125424.

(6) Stengel, M. Unified Ab Initio Formulation of Flexoelectricity and Strain-Gradient Elasticity. *Phys. Rev. B* **2016**, *93*, 245107.

(7) Mao, S.; Purohit, P. K. Insights Into Flexoelectric Solids From Strain-Gradient Elasticity. *J. Appl. Mech.* **2014**, DOI: 10.1115/1.4027451.

(8) Kogan, S. M. Piezoelectric Effect during Inhomogeneous Deformation and Acoustic Scattering of Carriers in Crystals. *Sov. Phys. Solid state* **1964**, *5*, 2069−2070.

(9) Tagantsev, A. K. Piezoelectricity and Flexoelectricity in Crystalline Dielectrics. *Phys. Rev. B* **1986**, *34*, 5883−5889.

(10) Yudin, P. V.; Tagantsev, A. K. Fundamentals of Flexoelectricity in Solids. *Nanotechnology* **2013**, *24*, 432001.

(11) Zubko, P.; Catalan, G.; Tagantsev, A. K. Flexoelectric Effect in Solids. *Annu. Rev. Mater. Res.* **2013**, *43*, 387−421.

(12) Nguyen, T. D.; Mao, S.; Yeh, Y. W.; Purohit, P. K.; McAlpine, M. C. Nanoscale Flexoelectricity. *Adv. Mater.* **2013**, *25*, 946−974.

(13) Ma, W.; Cross, L. E. Observation of the Flexoelectric Effect in Relaxor $Pb(Mg_{1/3}Nb_{2/3})O_3$ Ceramics. *Appl. Phys. Lett.* **2001**, *78*, 2920−2921.

(14) Ma, W.; Cross, L. E. Large Flexoelectric Polarization in Ceramic Lead Magnesium Niobate. *Appl. Phys. Lett.* **2001**, *79* (26), 4420−4422.

(15) Ma, W.; Cross, L. E. Flexoelectric Polarization of Barium Strontium Titanate in the Paraelectric State. *Appl. Phys. Lett.* **2002**, *81*, 3440−3442.

(16) Ma, W.; Cross, L. E. Flexoelectric Effect in Ceramic Lead Zirconate Titanate. *Appl. Phys. Lett.* **2005**, *86* (7), 72905.

(17) Ma, W.; Cross, L. E. Flexoelectricity of Barium Titanate. *Appl. Phys. Lett.* **2006**, *88* (23), 232902.

(18) Zubko, P.; Catalan, G.; Buckley, A.; Welche, P. R. L.; Scott, J. F. Strain-Gradient-Induced Polarization in $SrTiO_3$ Single Crystals. *Phys. Rev. Lett.* **2007**, *99*, 167601.
(19) Lee, D.; Yoon, A.; Jang, S. Y.; Yoon, J.-G.; Chung, J.-S.; Kim, M.; Scott, J. F.; Noh, T. W. Giant Flexoelectric Effect in Ferroelectric Epitaxial Thin Films. *Phys. Rev. Lett.* **2011**, *107* (5), 57602.
(20) Bhaskar, U. K.; Banerjee, N.; Abdollahi, A.; Wang, Z.; Schlom, D. G.; Rijnders, G.; Catalan, G. A Flexoelectric Microelectromechanical System on Silicon. *Nat. Nanotechnol.* **2016**, *11*, 263−266.
(21) Das, S.; Wang, B.; Paudel, T. R.; Park, S. M.; Tsymbal, E. Y.; Chen, L. Q.; Lee, D.; Noh, T. W. Enhanced Flexoelectricity at Reduced Dimensions Revealed by Mechanically Tunable Quantum Tunnelling. *Nat. Commun.* **2019**, *10*, 537.
(22) Dong, G.; Li, S.; Yao, M.; Zhou, Z.; Zhang, Y. Q.; Han, X.; Luo, Z.; Yao, J.; Peng, B.; Hu, Z.; Huang, H.; Jia, T.; Li, J.; Ren, W.; Ye, Z. G.; Ding, X.; Sun, J.; Nan, C. W.; Chen, L. Q.; Li, J.; Liu, M. Super-Elastic Ferroelectric Single-Crystal Membrane with Continuous Electric Dipole Rotation. *Science* **2019**, *366* (6464), 475−479.
(23) Peng, B.; Peng, R.-C.; Zhang, Y.-Q.; Dong, G.; Zhou, Z.; Zhou, Y.; Li, T.; Liu, Z.; Luo, Z.; Wang, S.; Xia, Y.; Qiu, R.; Cheng, X.; Xue, F.; Hu, Z.; Ren, W.; Ye, Z.-G.; Chen, L.-Q.; Shan, Z.; Min, T.; Liu, M. Phase Transition Enhanced Superior Elasticity in Freestanding Single-Crystalline Multiferroic $BiFeO_3$ Membranes. *Sci. Adv.* **2020**, *6* (34), eaba5847.
(24) Bakaul, S. R.; Kim, J.; Hong, S.; Cherukara, M. J.; Zhou, T.; Stan, L.; Serrao, C. R.; Salahuddin, S.; Petford-Long, A. K.; Fong, D. D.; Holt, M. V. Ferroelectric Domain Wall Motion in Freestanding Single-Crystal Complex Oxide Thin Film. *Adv. Mater.* **2020**, *32* (4), 1907036.
(25) Guo, R.; You, L.; Lin, W.; Abdelsamie, A.; Shu, X.; Zhou, G.; Chen, S.; Liu, L.; Yan, X.; Wang, J.; Chen, J. Continuously Controllable Photoconductance in Freestanding BiFeO3 by the Macroscopic Flexoelectric Effect. *Nat. Commun.* **2020**, *11* (1), 2571.
(26) Cross, L. E. Flexoelectric Effects: Charge Separation in Insulating Solids Subjected to Elastic Strain Gradients. *J. Mater. Sci.* **2006**, *41*, 53−63.
(27) Chu, B.; Zhu, W.; Li, N.; Cross, L. E. Flexure Mode Flexoelectric Piezoelectric Composites. *J. Appl. Phys.* **2009**, *106* (10), 104109.
(28) Cordero-Edwards, K.; Domingo, N.; Abdollahi, A.; Sort, J.; Catalan, G. Ferroelectrics as Smart Mechanical Materials. *Adv. Mater.* **2017**, *29*, 1702210.
(29) Warner, A. W.; Onoe, M.; Coquin, G. A. Determination of Elastic and Piezoelectric Constants for Crystals in Class (3m). *J. Acoust. Soc. Am.* **1967**, *42* (6), 1223−1231.
(30) Lu, D.; Baek, D. J.; Hong, S. S.; Kourkoutis, L. F.; Hikita, Y.; Hwang, H. Y. Synthesis of Freestanding Single-Crystal Perovskite Films and Heterostructures by Etching of Sacrificial Water-Soluble Layers. *Nat. Mater.* **2016**, *15* (12), 1255−1260.
(31) Hong, S. S.; Gu, M.; Verma, M.; Harbola, V.; Wang, B. Y.; Lu, D.; Vailionis, A.; Hikita, Y.; Pentcheva, R.; Rondinelli, J. M.; Hwang, H. Y. Extreme Tensile Strain States in $La_{0.7}Ca_{0.3}MnO_3$ Membranes. *Science* **2020**, *368* (6486), 71−76.
(32) Gan, Q.; Rao, R. A.; Eom, C. B.; Garrett, J. L.; Lee, M. Direct Measurement of Strain Effects on Magnetic and Electrical Properties of Epitaxial SrRuO3 Thin Films. *Appl. Phys. Lett.* **1998**, *72* (8), 978−980.
(33) Xu, R.; Huang, J.; Barnard, E. S.; Hong, S. S.; Singh, P.; Wong, E. K.; Jansen, T.; Harbola, V.; Xiao, J.; Wang, B. Y.; Crossley, S.; Lu, D.; Liu, S.; Hwang, H. Y. Strain-Induced Room-Temperature Ferroelectricity in $SrTiO_3$ Membranes. *Nat. Commun.* **2020**, *11* (1), 3141.
(34) Mudinepalli, V. R.; Feng, L.; Lin, W.-C.; Murty, B. S. Effect of Grain Size on Dielectric and Ferroelectric Properties of Nanostructured $Ba_{0.8}Sr_{0.2}TiO_3$ Ceramics. *J. Adv. Ceram* **2015**, *4* (1), 46−53.
(35) Pesquera, D.; Parsonnet, E.; Qualls, A.; Xu, R.; Gubser, A. J.; Kim, J.; Jiang, Y.; Velarde, G.; Huang, Y.-L.; Hwang, H. Y.; Ramesh, R.; Martin, L. W. Beyond Substrates: Strain Engineering of Ferroelectric Membranes. *Adv. Mater.* **2020**, *32* (43), 2003780.
(36) Bakaul, S. R.; Serrao, C. R.; Lee, M.; Yeung, C. W.; Sarker, A.; Hsu, S. L.; Yadav, A. K.; Dedon, L.; You, L.; Khan, A. I.; Clarkson, J. D.; Hu, C.; Ramesh, R.; Salahuddin, S. Single Crystal Functional Oxides on Silicon. *Nat. Commun.* **2016**, *7*, 10547.
(37) Poot, M.; Van Der Zant, H. S. J. Nanomechanical Properties of Few-Layer Graphene Membranes. *Appl. Phys. Lett.* **2008**, *92*, 63111.
(38) Lee, C.; Wei, X.; Kysar, J. W.; Hone, J. Measurement of the Elastic Properties and Intrinsic Strength of Monolayer Graphene. *Science* **2008**, *321*, 385−388.
(39) Castellanos-Gomez, A.; Poot, M.; Steele, G. A.; Van Der Zant, H. S. J.; Agraït, N.; Rubio-Bollinger, G. Elastic Properties of Freely Suspended MoS_2 Nanosheets. *Adv. Mater.* **2012**, *24*, 772−775.
(40) Harbola, V.; Xu, R.; Crossley, S.; Singh, P.; Hwang, H. Y. Fracture and Fatigue of Thin Crystalline $SrTiO_3$ Membranes. *Appl. Phys. Lett.* **2021**, *119* (5), 53102.
(41) Xu, R.; Crust, K. J.; Harbola, V.; Arras, R.; Patel, K. Y.; Prosandeev, S.; Cao, H.; Shao, Y.-T.; Behera, P.; Caretta, L.; Kim, W. J.; Khandelwal, A.; Acharya, M.; Wang, M. M.; Liu, Y.; Barnard, E. S.; Raja, A.; Martin, L. W.; Gu, X. W.; Zhou, H.; Ramesh, R.; Muller, D. A.; Bellaiche, L.; Hwang, H. Y. Size-Induced Ferroelectricity in Antiferroelectric Oxide Membranes. *Adv. Mater.* **2023**, *35* (17), 2210562.
(42) Cook, S. M.; Schäffer, T. E.; Chynoweth, K. M.; Wigton, M.; Simmonds, R. W.; Lang, K. M. Practical Implementation of Dynamic Methods for Measuring Atomic Force Microscope Cantilever Spring Constants. *Nanotechnology* **2006**, *17*, 2135−2145.
(43) Cheng, B. L.; Gabbay, M.; Duffy, W.; Fantozzi, G. Mechanical Loss and Young's Modulus Associated with Phase Transitions in Barium Titanate Based Ceramics. *J. Mater. Sci.* **1996**, *31* (18), 4951−4955.
(44) Dong, L.; Stone, D. S.; Lakes, R. S. Softening of Bulk Modulus and Negative Poisson Ratio in Barium Titanate Ceramic near the Curie Point. *Philos. Mag. Lett.* **2010**, *90* (1), 23−33.
(45) Berlincourt, D. A.; Kulcsar, F. Electromechanical Properties of BaTiO3 Compositions Showing Substantial Shifts in Phase Transition Points. *J. Acoust. Soc. Am.* **1952**, *24* (6), 709−713.
(46) Wang, W.; Liu, D.; Zhang, Q.; Ren, B.; Zhang, Y.; Jiao, J.; Lin, D.; Zhao, X.; Luo, H. Shear-Mode Piezoelectric Properties of Ternary $Pb(In_{1/2}Nb_{1/2})O_3$−$Pb(Mg_{1/3}Nb_{2/3})O_3$−$PbTiO_3$ Single Crystals. *J. Appl. Phys.* **2010**, *107* (8), 84101.

https://doi.org/10.1021/acs.nanolett.4c02946
Nano Lett. 2024, 24, 10331−10336